# Evaluation of Kelvin probe force microscopy for imaging grain boundaries in chalcopyrite thin films

C. Leendertz, F. Streicher, M. Ch. Lux-Steiner, and S. Sadewasser[a)]
*Department of Solar Energy, Hahn-Meitner Institut Berlin, Glienicker Str. 100, D-14109 Berlin, Germany*

(Received 26 June 2006; accepted 26 July 2006; published online 15 September 2006)

In view of the outstanding performance of polycrystalline thin film solar cells on the basis of $Cu(In,Ga)Se_2$, the electrical activity at grain boundaries currently receives considerable attention. Recently, Kelvin probe force microscopy (KPFM) has been applied to characterize the properties of individual grain boundaries, observing a drop in the work function in many cases. We present finite element simulations of the electrostatic forces to assess the experimental resolution of KPFM. Depending on the tip-sample distance, the observed drop in the work function amounts to only a fraction of the real potential drop. The simulations are considered for different grain boundary models and consequences for the quantitative evaluation of experimental results are discussed. © *2006 American Institute of Physics*. [DOI: 10.1063/1.2354474]

Currently, the role of grain boundaries (GBs) in polycrystalline chalcopyrite thin film solar cells is intensely discussed. The interest in the topic is largely motivated by the fact that solar cell devices based on polycrystalline $Cu(In,Ga)Se_2$ thin films exhibit high power conversion efficiencies despite the presence of grain boundaries. In Hall measurements an activated behavior of the mobility was observed, giving a barrier for majority carrier transport at the GB of 60–135 meV.[1] Additional insight was gained by studying individual GBs using microscopic techniques such as Kelvin probe force microscopy (KPFM),[2–5] scanning tunneling microscopy,[6,7] (STM) and cathodoluminescence in a scanning or transmission electron microscope.[8,9] Various KPFM experiments observed a drop in the work function between 0 and 150 meV, depending on the Ga concentration[5] and film texture.[9] When assigned to GB charges, these potential drops would correspond to a barrier for hole transport leading to hole repulsion from the GB. Barriers for electron transport have been observed by electroassisted STM.[7]

Initially, the properties of GBs in chalcopyrite semiconductors were discussed considering a GB model developed for polycrystalline Si.[1,10] Charged defects at the GB result in band bending, which extends into the grain interior and presents a barrier for charge transport; in the case of *p*-type $Cu(In,Ga)Se_2$ donorlike traps result in downward band bending and a barrier for majority carrier transport, see Fig. 1(a). In contrast to this electronic GB model, another, recently proposed model is based on structural considerations. A valence band offset $\Delta E_V$ at GBs of $CuInSe_2$ is predicted, resulting in effective hole repulsion and thereby a reduced recombination at the GB.[11] The tendency for $(2V_{Cu}^{-}+In_{Cu}^{2+})$ defect complex formation at polar (112) surfaces[12] was assumed to occur also at (112) GBs, thus leading to a corresponding $\Delta E_V$. For the case of $CuGaSe_2$ also a conduction band offset $\Delta E_C \approx 0.5$ eV was predicted, see Fig. 1(b).[13] These considerations are very specific for the (112) GBs and might not apply to other GB orientations possibly present in polycrystalline absorber material.

In this letter we evaluate the spatial resolution of KPFM with respect to its capability to distinguish the existing GB models based on the measurement of the drop in the contact potential at GBs. Consequences for the quantitative evaluation of KPFM experiments on GBs are discussed and optimized experimental conditions are proposed.

The detection principle of KPFM is based on the sensitivity of the tip and cantilever to electrostatic forces.[14,15] These forces have a long range character resulting in an averaging effect: not only the outermost end of the tip is relevant for the detection of the electrostatic forces but regions of the tip cone and to some extent also the cantilever itself contribute to the total force sensed by the cantilever. The contact potential is obtained by minimizing the electrostatic forces; thus, a weighted average of the contact potentials in a certain region below the tip is obtained.[16–18]

We have applied three dimensional finite element methods to simulate the electrostatic field of the tip-sample geometry, assuming a flat sample topography. The tip potential to minimize the electrostatic forces is deduced for each position of the tip on the sample. The metallic tip is assigned a potential $V_{tip}$ and the typical values of a commercial tip geometry (Nanosensors, EFM, tip radius=20 nm, cone half opening angle=20°, tip height=13 $\mu$m, and cantilever width =25 $\mu$m) are used. The sample is modeled by a flat metallic plate to which a diplike potential is assigned, depending on

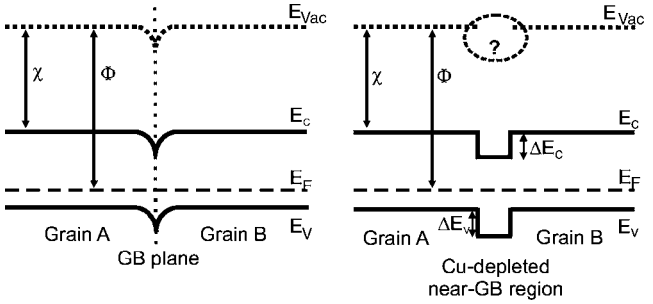


FIG. 1. Different models for GBs in polycrystalline $Cu(In,Ga)Se_2$ films. (a) Charged defects at the GB result in a band bending and (b) the structural properties of the (112) GB surface result in conduction and valence band offsets. The profile of the local vacuum level has not yet been predicted. Adapted from Ref. 3.

[a)]Electronic mail: sadewasser@hmi.de

 

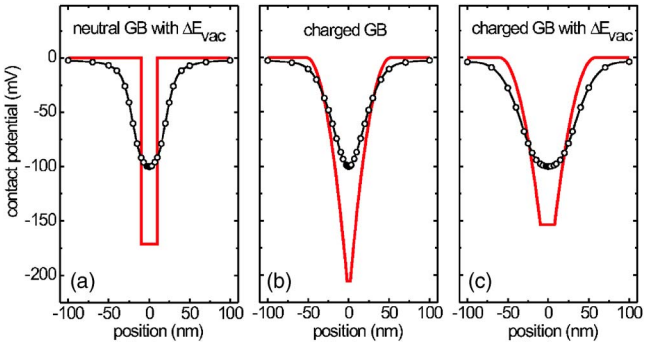


FIG. 2. (Color online) Simulations of KPFM measurements for different GB models. (a) A vacuum level discontinuity $\Delta E_{vac}$, (b) a GB with charged defects resulting in a 50 nm wide space charge region, and (c) a combination of vacuum level discontinuity with charged GB defects. The solid lines represent the input to the simulation and the points the simulated KPFM profile.

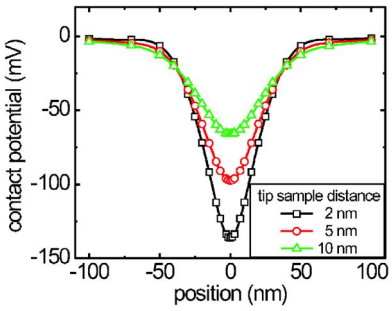


FIG. 3. (Color online) Simulations of KPFM measurements at different tip-sample distance for a charged grain boundary.

the implemented grain boundary model (see below). For a given position of the tip, the Poisson equation is solved and the electrostatic force $F_{el}$ extracted. The procedure is repeated for different values of $V_{tip}$; $F_{el}(V_{tip})$ shows the expected parabolic dependence, which is fitted to extract the minimum, corresponding to the contact potential. The whole procedure is repeated for 25 tip positions across the GB, leading to a simulated line profile across the grain boundary. In addition, the tip-sample distance was varied between 2 and 10 nm, values typically used in experimental KPFM scans.

To consider the different grain boundary models, we evaluate three cases: (i) a charge-neutral grain boundary with a discontinuity in the vacuum level $\Delta E_{vac}$ due to an interface dipole, (ii) a GB potential due to charged defects at the GB, $\Delta\Phi_{GB}$, and (iii) a combination of both $\Delta E_{vac}$ and $\Delta\Phi_{GB}$. The input to the simulations (namely, the situation at the GB) is shown by the solid lines in Figs. 2(a)–2(c), respectively. Experimentally, a drop in the contact potential has been observed[2–5,9] and in view of the structural model, which predicts band offsets in valence and conduction bands, the only possibility to explain the observed KPFM experiments with this model is due to an offset in the vacuum level stemming from an interface dipole at the transition from the Cu-depleted grain boundary phase to the grain interior phase. Since a typical dip of $\approx$100 mV is found in KPFM experiments, the input to the simulations was selected such that the simulated KPFM profile results in a dip depth of 100 mV for all three cases. In Fig. 2(a) a vacuum level discontinuity $\Delta E_{vac}$=171 meV is modeled by a 20 nm wide rectangular drop in the contact potential. The simulated KPFM profile (points) results in a broadened dip with a considerably lower dip depth (58% of the input depth). For the case of a GB with charged defects, a space-charge-like dip $\Delta\Phi_{GB}$ =205 mV with 50 nm space charge regions is used as the input for the simulations [Fig. 2(b)]. The simulated KPFM profile (points) results to a dip depth 49% of the input with a dip shape that appears similar to the shape of the input space charge region. The combination of vacuum level discontinuity and charged GB defects is shown in Fig. 2(c). The simulated KPFM measurement reaches 65% of the input dip depth. The simulated KPFM profiles for all three cases resemble each other quite closely, especially when experimental noise is considered, which in reported measurements ranges between 5 mV (Refs. 2 and 3) and 50 mV.[4]

The influence of the tip-sample distance on the simulated KPFM line profile is shown in Fig. 3 for the case of a charged grain boundary with a dip depth of 200 mV. It is seen that the simulated dip depth is better reproducing the input, the closer the tip is to the sample; this is intuitive as for closer tip-sample distance the relative contribution of the outermost tip end is increased.

The presented simulations lead to the conclusion that based on KPFM experiments alone it will be very difficult to favor one model over another, at least if only measurements under dark conditions are considered. Nevertheless, KPFM measurements under illumination can shed more light on the issue. Under super-band-gap illumination, electron-hole pairs are generated, which can be separated in internal electric fields, as, for example, present at surfaces or at GBs (due to charged defects). The difference in work function between illuminated and dark conditions is defined as the surface photovoltage (SPV). In the case of charged GB defects, an additional $SPV_{GB}$ can result with respect to the SPV on the grain surface. For the GB model, considering only a neutral $\Delta E_{vac}$ no charge separation at the GB would result and consequently no $SPV_{GB}$ would be observed. Therefore, despite the similarities of the simulated KPFM profiles across GBs, KPFM experiments under illumination can give important information to gain more insight into the GB physics in chalcopyrite materials.

This has been experimentally shown in Refs. 2 and 3 and is shown in Fig. 4, reproduced from Ref. 3. The upper panel shows a line profile across two grain boundaries of a $CuGaSe_2$ thin film measured in the dark and under monochromatic super-band-gap illumination. The difference between the two profiles gives the SPV and is presented in the lower panel. Clearly, grain boundary B shows an elevated SPV compared to the grain surfaces and grain boundary A. This $SPV_{GB}$ can only be explained by a charged grain boundary.

The KPFM experiments image the potential dip at grain boundaries providing also information about the width of the potential dip. From Fig. 2 it is seen that even though the dip depth is reduced to about 50%, the width of the dip is reproduced fairly well. From these values the charge at the grain boundary and the net doping of the absorber can be estimated,[1,2,19] using $P_{GB}=(1/e)\sqrt{8\epsilon\epsilon_0 P_{net}\Delta\Phi_{GB}}$ and $P_{net}=2\epsilon\epsilon_0\Delta\Phi_{GB}/e^2w^2$, respectively. The simulation suggests that the KPFM experiments underestimate the dip depth by about 50%, thus $P_{GB}$ and $P_{net}$ are also underestimated by about 50%. For the potential drop at the GBs observed in Ref. 2 this results in $P_{GB}=1.6\times10^{12}$ cm$^{-2}$ and $P_{net}=1.8$

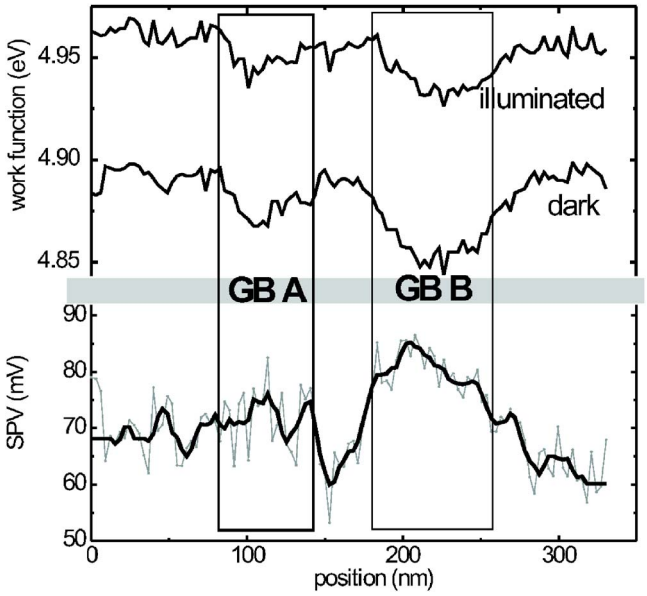


FIG. 4. (Color online) Line profile across two grain boundaries of a $CuGaSe_2$ thin film obtained by peel off from a Mo/glass substrate. The upper panel shows a drop in the work function (in darkness and under illumination) at the position of the GBs. Grain boundaries A and B show a different SPV characteristic (lower panel); the line is a smoothed curve of the data (gray line). Reproduced from Ref. 3.

$\times 10^{17}$ $cm^{-3}$, which is in excellent agreement with the values obtained from Hall measurements obtained on the same samples.[1]

The dependence of the dip depth on the tip-sample distance, as shown in Fig. 3, suggests that for optimized experimental results a close tip-sample distance should be selected. Considering that in many experiments the surface of the polycrystalline thin films is comparably rough, showing height differences of up to several hundreds of nanometers, a small tip-sample distance is experimentally difficult to realize. Therefore, quantitative evaluation of KPFM experiments on grain boundaries has to be considered carefully, preferably taking simulations into account. In the future we plan to include the sample topography in the simulation, in order to study its effect on the simulation results.

In conclusion we have presented finite element simulations of the electrostatic fields in KPFM, showing that KPFM experiments image a reduced dip depth for the contact potential change at grain boundaries in chalcopyrite semiconductors. This leads to underestimated grain boundary charge and net carrier concentrations. Optimized KPFM experiments should intend to minimize the tip-sample distance.

The authors acknowledge financial support from the Deutsche Forschungsgemeinschaft.

[1] S. Schuler, S. Nishiwaki, J. Beckmann, N. Rega, S. Brehme, S. Siebentritt, and M. Ch. Lux-Steiner, *29th IEEE Photovoltaic Specialist Conference* (IEEE, New Orleans, LA, 2002), p. 504.
[2] S. Sadewasser, Th. Glatzel, S. Schuler, S. Nishiwaki, R. Kaigawa, and M. Ch. Lux-Steiner, Thin Solid Films **431–432**, 257 (2003).
[3] D. Fuertes Marrón, S. Sadewasser, Th. Glatzel, A. Meeder, and M. Ch. Lux-Steiner, Phys. Rev. B **71**, 033306 (2005).
[4] C.-S. Jiang, R. Noufi, J. A. AbuShama, K. Ramanathan, H. R. Moutinho, J. Pankow, and M. M. Al-Jassim, Appl. Phys. Lett. **84**, 3477 (2004).
[5] C.-S. Jiang, R. Noufi, K. Ramanathan, J. A. AbuShama, H. R. Moutinho, and M. M. Al-Jassim, Appl. Phys. Lett. **85**, 2625 (2004).
[6] M. J. Romero, C.-S. Jiang, R. Noufi, and M. Al-Jassim, Appl. Phys. Lett. **86**, 143115 (2005).
[7] M. J. Romero, C.-S. Jiang, R. Noufi, and M. Al-Jassim, Appl. Phys. Lett. **87**, 172106 (2005).
[8] M. J. Romero, K. Ramanathan, M. A. Contreras, M. M. Al-Jassim, R. Noufi, and P. Sheldon, Appl. Phys. Lett. **83**, 4770 (2003).
[9] G. Hanna, Th. Glatzel, S. Sadewasser, N. Ott, H. P. Strunk, U. Rau, and J. H. Werner, Appl. Phys. A: Mater. Sci. Process. **82**, 1 (2006).
[10] J. Y. W. Seto, J. Appl. Phys. **46**, 5247 (1975).
[11] C. Persson and A. Zunger, Phys. Rev. Lett. **91**, 266401 (2003).
[12] S. B. Zhang and S.-H. Wei, Phys. Rev. B **65**, 081402(R) (2002).
[13] C. Persson and A. Zunger, Appl. Phys. Lett. **87**, 211904 (2005).
[14] J. M. R. Weaver and D. W. Abraham, J. Vac. Sci. Technol. B **9**, 1559 (1991); M. Nonnenmacher, M. P. O'Boyle, and H. K. Wickramasinghe, Appl. Phys. Lett. **58**, 2921 (1991).
[15] Ch. Sommerhalter, Th. W. Matthes, Th. Glatzel, A. Jäger-Waldau, and M. Ch. Lux-Steiner, Appl. Phys. Lett. **75**, 286 (1999).
[16] T. Hochwitz, A. K. Henning, C. Levey, C. Daghlian, and J. Slinkman, J. Vac. Sci. Technol. B **14**, 457 (1996).
[17] J. Colchero, A. Gil, and A. M. Baró, Phys. Rev. B **64**, 245403 (2001).
[18] S. Belaidi, F. Lebon, P. Girard, G. Leveque, and S. Pagano, Appl. Phys. A: Mater. Sci. Process. **66**, S239 (1998).
[19] D. Fuertes Marrón, A. Meeder, S. Sadewasser, R. Würz, C. A. Kaufmann, Th. Glatzel, Th. Schedel-Niedrig, and M. Ch. Lux-Steiner, J. Appl. Phys. **97**, 094915 (2005).